Journal of Materials Chemistry A

Accepted Manuscript

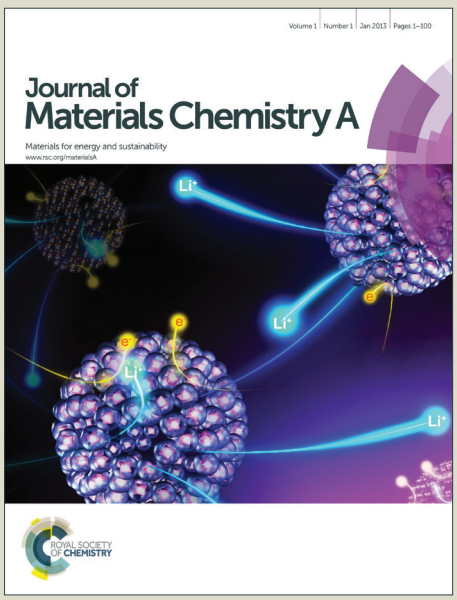

ROYAL SOCIETY OF CHEMISTRY

www.rsc.org/materialsA

Journal Name

RSCPublishing

ARTICLE

Construction and adsorption properties of Porous Aromatic Frameworks via $AlCl_3$-triggered Coupling Polymerization

Lina Li, Hao Ren*, Ye Yuan, Guangli Yu and Guangshan Zhu

Cite this: DOI: 10.1039/x0xx00000x

Received 00th January 2012,
Accepted 00th January 2012

DOI: 10.1039/x0xx00000x

www.rsc.org/

Currently, synthesis of most porous organic frameworks (POFs) requires noble metals as main catalyst. Herein we report a low-cost and straightforward synthetic strategy to develop porous aromatic frameworks (PAF). With $AlCl_3$ as catalyst, the Scholl coupling reaction could occur between the phenyl rings of aromatic compounds. Using 3-dimensional monomers, such as triphenylamine, tetraphenylmethane, tetraphenylsilane, and tetraphenlgermane, we successfully obtained a series of PAFs with moderate Brunauer–Emmett–Teller (BET) surface areas ranging from 515 $m^2 g^{-1}$ to 1119 $m^2 g^{-1}$. Among the obtained PAF materials, PAF-41 exhibited the best CH_4 and CO_2 sorption capacity with CH_4 (1.04 mmol g^{-1}) and CO_2 (3.52 mmol g^{-1}) at 273 K. In addition, PAF-43 demonstrated its comparably high isosteric heat of adsorptions at 34.8 kJ mol^{-1} for CO_2 and 29.7 kJ mol^{-1} for CH_4. It is also worth mentioning that the developed approach also overcome typical flaws of some classic PAFs, such as high cost and complexity of precursor preparation.

Introduction

Porous organic frameworks (POFs) are a series of designable polymers with rigid structural networks and inherent porosities[1-4]. The attractive advantages of POFs include large specific surface areas, high chemical and thermal stabilities, and low skeleton density, etc[5]. Various POFs, such as covalent organic frameworks (COFs)[6-8], polymers of intrinsic microporosity (PIMs)[9], conjugated microporous polymers (CMPs)[10], hyper-crosslinked polymers (HCPs)[11], triazine-based organic frameworks (CTFs)[12,13], and porous aromatic frameworks (PAFs)[5,14], have been successfully designed and synthesized in the past decade, and as a result, they have brought major advances in porous materials domain. Besides, these materials have been studied extensively as a series of new porous materials owing to their controllable pores and potential applications in fields of gas adsorption[15], gas storage and separation[16], heterogeneous catalysis[16-17], sensors[18,19] and electricity[20].

Recently, most of POF materials are obtained in solution system[5a,18]. Besides, ionothermal[12,14a] and Mechanochemical[5b,5c] strategies have been proposed for synthesis of POFs. Various reaction methods greatly boost the prosperity of POF materials. In POFs synthesis, there are several pioneering and effective coupling strategies, such as Suzuki coupling reaction[21], and Sonogashira–Hagihara coupling reaction[10], Yamamoto reaction[5,22], ethynyl trimerization reaction[23], carbazole-based coupling polymerization[24], etc. However, most of the above routes requires palladium and nickel (0) compounds as catalyst, which are expensive and oxygen-sensitive. In addition, corresponding monomers are strictly limited to the ones having special functional groups, such as —Br, —$B(OH)_2$, —C≡C, —C=C, which are relatively difficult to prepare. Therefore, most of these methods suffer from one or more of the following limitations: requirement of drastic synthetic conditions, tedious purifications, difficulties in reproducing results, multistep synthesis from the aromatic hydrocarbon precursor, and the formation of gross mixtures due to competing reactions. In other words, the traditional methods of constructing POFs are not only complicated but also expensive, thereby making them difficult in case of mass production. Recently, Friedel-Crafts reaction has been reported as an effective strategy for preparation of POFs. Even this practice still requires electron-donating groups or linkers (e.g. formaldehyde dimethyl acetal), the introduction of Friedel-Crafts reaction promotes the development of POFs[24,25].

In fact, aromatic monomers can also be directly coupled by other means. As documented, with the help of Lewis acid[26], aromatic nucleus of monomer are activated to achieve polymerizations to produce homo-polymers. Therefore, multiple-phenyl product can be prepared in high yield by a simple, one-step procedure involving treatment of phenyl rings with cupric chloride and ferric chloride[26]. Herein, we adopted

an easy and low cost strategy to achieve POF materials, using $AlCl_3$-induced Scholl reaction. Furthermore, a series of PAF materials, referred to as PAF-41, PAF-42, PAF-43, and PAF-44, were obtained with moderate BET surface areas ranging from 515 $m^2 g^{-1}$ to 1119 $m^2 g^{-1}$. Among those samples, PAF-41 revealed a superior sorption capacity with CH_4 (1.04 mmol g^{-1}) and CO_2 (3.52 mmol g^{-1}) at 273 K, while PAF-43 demonstrated great performance with the isosteric heat of adsorption at 35 kJ mol^{-1} for CO_2 and 29.7 kJ mol^{-1} for CH_4.

Experiment

Instruments

The FTIR spectra were measured as KBr pellets using IFS 66V/S Fourier transform infrared spectrometer. The thermalgravimetric analysis (TGA) was performed using a TA model TGA Q500 thermal analyzer system up to 800 °C under air atmosphere at a heating rate of 5 °C min^{-1}. The SEM analysis was carried out on a JEOL model JSM-6700F scanning electron microscope and Iridium (IXRF Systems) software with an accelerating voltage of 5 kV. Field emission transmission electron microscopy (TEM) was performed on a FEI Tecnai G2 F20 S-TWIN transmission electron microscope. N_2 adsorption isotherms were measured on Quantachrome Autosorb-1C analyzer. CO_2 and CH_4 sorption adsorption isotherms at 273 K and 298 K were measured on a Quantachrome Autosorb iQ2 analyzer, respectively.

Materials

Tetraphenylmethane, tetraphenylsilane and tetraphenylgermane were received from Alfa Aesar. Triphenylamine and anhydrous aluminium chloride were received from Aladdin Reagent. Chloroform was dried over 4 A molecular sieve before employment.

Synthesis of PAF materials

The synthesis of PAF-41, PAF-42, PAF-43, and PAF-44 are carried out with $AlCl_3$ as catalysis, based on previous reports of Kovacic[26] and the work of Scholl and Seer[27]. After several attempts, a typical synthesis and purification procedure for PAF-42 is described in detail as follows, while similar synthesis processes of PAF-41, PAF-43, and PAF-44 are seen in supporting information.

Firstly, anhydrous aluminium chloride (500 mg, 3.75 mmol) was added to a 100 mL round-bottomed flask. Then, after pumped to vacuum, the system was trice inflated with inert gas (N_2). Next, dried chloroform (40 mL) was injected through a syringe and the mixture was heated to 60 °C for 3 h. To the resulting brown solution, tetraphenylmethane (1.5 mmol, 480 mg) in 20 mL $CHCl_3$ was added into the system and mixture was stirred at 60 °C for 24 h. After cooling down to room temperature, the crude product was obtained by filtration and washed with 1 M hydrochloric acid solution, methanol, and acetone to remove unreacted monomers and catalyst residues. Further purification of product was carried out by Soxhlet extraction with ethanol, THF, and $CHCl_3$ in turns for 48 h. The product was dried in vacuum for 8 h at 80 °C to obtain PAF-42 (469 mg, 98.6% yield).

Results and discussion

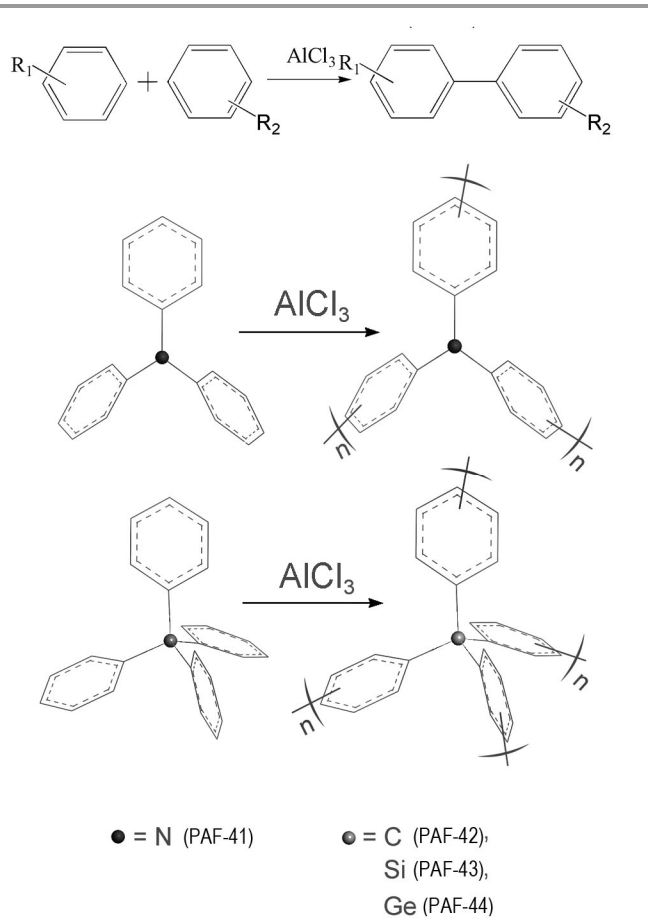

Figure 1. Cross-coupling reaction to obtain extended frameworks.

In the synthesis of POF materials, suitable reactions and reasonable building blocks are two critical issues to take into consideration. Currently, several noble metal catalyzed reactions have been documented for effective preparation of POFs. To explore an easy and low cost strategy for POF-material synthesis, we select Lewis acid $AlCl_3$ for aromatic homo-polymers preparation. This simple synthetic procedure mainly proceeds through the generations of protons, produced from $AlCl_3$ and trace amounts of H_2O in $CHCl_3$, which impact and activate the benzene rings. Subsequently, activated monomers were able to attack inactivated ones in the system, resulting in C-C coupling among aromatic molecules. Moreover, in order to obtain porous structures, 3-dimensional monomers were selected, such as triphenylamine, tetraphenylmethane, tetraphenylsilane, and tetraphenylgermane.

The structures of obtained PAF materials are firstly studied using FTIR spectroscopy. Figure 2 and Figure S1 show IR spectra of the PAF samples and corresponding monomers. After Scholl reaction, the absorption peaks of C-H and C-C in 1650-1400 cm^{-1} region and 800-700 cm^{-1} of the benzene ring obviously vary both in terms of position and intensity (Figure 2). These changes of characteristic absorption peaks are analyzed as follows (Table S2): 1, the peaks at 770-730 cm^{-1} belong to the C-H deformation vibration of five adjacent ring hydrogens., intensity of these peaks are obviously weakened (Figure 2) owing to the reduction of adjacent ring hydrogens (from five to four); 2, ring deformation vibration of mono-substituted benzene experienced a pronounced reduction in 715-690 cm^{-1} band due to the disubstitution of benzene rings;

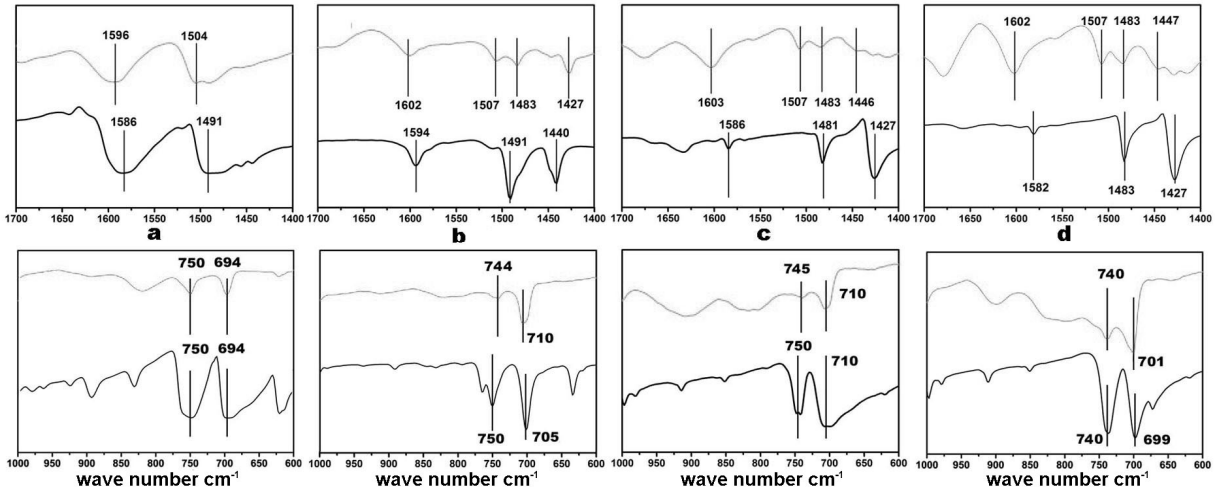

Figure 2. IR spectra of PAF-41(a, grey), PAF-42(b), PAF-43(c), PAF-44 (d) and their corresponding monomers (black) in the ranges of 1700 cm^{-1} to 1400 cm^{-1} and 1000 cm^{-1} to 600 cm^{-1}.

3, the C-C stretching vibration bands of monosubstituted benzenes are usually at around 1490 cm^{-1}, whereas those of 1,4-disubstituted benzenes are at around 1512 cm^{-1}. In other words, monomers associated peaks were red shifted after the coupling reaction. To be specific, the peaks at 1490 cm^{-1} (PAF-41), 1481 cm^{-1} (PAF-43) and 1483 cm^{-1} (PAF-44) were replaced by the ones at about 1507 cm^{-1}, which demonstrated that substitution transpired at para-position; 4, another group of C-C stretching vibration peaks of monosubstituted benzenes are found at about 1585, while peaks of bi-substituted benzenes were detected at 1605, which coincides with the experiment results. The peaks of monomers (around 1590 cm^{-1}) were red shifted in PAF-42 (1602 cm^{-1}), PAF-43 (1603 cm^{-1}), and PAF-44 (1602 cm^{-1}). All monomers specific peaks were replaced by new peaks due to substitution reactions. Also, peak of PAF-42 at 1491 cm^{-1} is divided into two prominent peaks at 1507 and 1483 cm^{-1} respectively, pointing out para and ortho substitutions.

Furthermore, solid-state ^{13}C CP/MAS NMR studies were performed to reveal the local structures of these polymer networks. According to Figure 3, there were two prominent peaks in the range of 120–140 ppm, which were related to aromatic carbon atoms of building phenyl ring units. As reported earlier[5,14b], the intense signals at d=132 ppm could be assigned to unsubstituted phenyl carbons, while the relatively weaker signals at d=146 ppm were attributed to substituted phenyl carbons. Additionally, the quaternary carbon atom in PAF-42 can be confirmed by peak at around 64 ppm. All these findings prove the occurrence of coupling reactions.

Powder X-ray diffraction (PXRD) and transmission electron microscopy (TEM) was used to investigate the crystallinity and regularity of resulting PAFs. The PXRD pattern illustrates the amorphous nature of as synthesized PAFs (Figure S3). Disordered linkages among the building units of frameworks are due to the distortion of the phenyl rings and substitution of para-position and ortho-position. From the TEM analysis (Fig. S4), an ordered and obvious pore structure could not be found, indicating their amorphous textures. Based on scanning electron microscopy (SEM) (Figure 4) and TEM investigations, it can be inferred that the powder PAF have a deformed spherical morphology, with dimensions ranging from 200-800 nm.

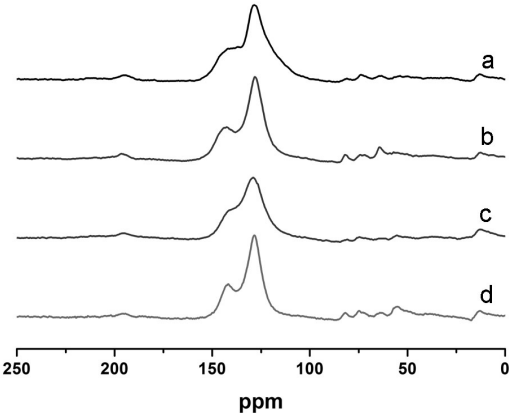

Figure 3. ^{13}C CP/MAS NMR spectra of PAF-41 (a), PAF-42 (b), PAF-43 (c), and PAF-44 (d).

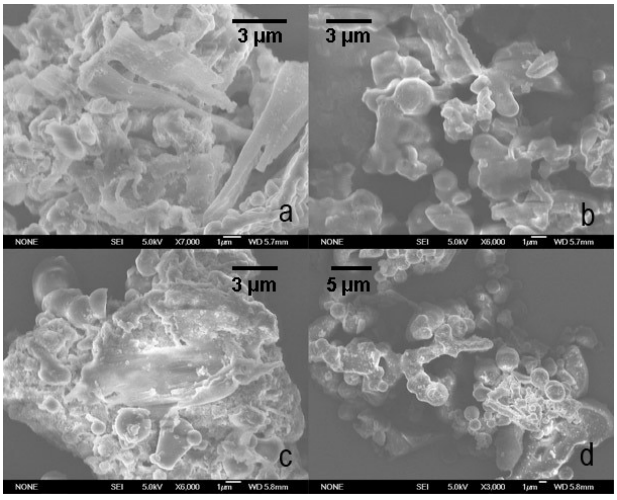

Figure. 4. SEM images of PAF-41 (a), PAF-42 (b), PAF-43 (c) and PAF-44 (d).

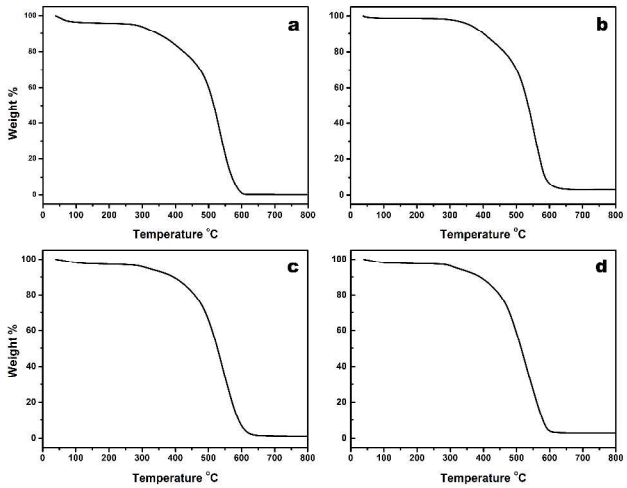

Figure 5. TGA curves of PAF-41 (a), PAF-42 (b), PAF-43 (c), and PAF-44 (d).

The thermal stability of these products was studied with thermogravimetric analysis (TGA). As shown in Figure 5, the weight of these polymers was slowly reduced before 300 °C and the framework decomposition of PAFs started over 400 °C, revealing a high thermal stability of organic polymers. In addition, all PAF materials were purified with Soxhlet extraction using low boiling point solvents (ethanol, THF, and $CHCl_3$). Besides, these polymers have also been tested in other common solvents (DMF, DMSO and NMP) and 1 M HCl acid solution. These PAF materials could not be dissolved or reduced after immersing in these solvents and 1 M HCl acid for a long time, indicating they are chemical stably.

The porosities of PAF materials were tested using nitrogen sorption isotherms at 77 K. All samples exhibit classical type I isotherm featured by a sharp uptake at the low-pressure region (Figure 6). Besides, they display a distinct hysteresis extending to low pressure between the adsorption and desorption cycles, which is commonly observed in many POF networks[14b,28]. The apparent surface areas are calculated from the BET and Langmuir models. Encouragingly, the BET surface area of PAF-41, utilizing TPA as building units, reaches 1119 m^2 g^{-1}, which almost double that of PAF-42, PAF-43, and PAF-42. The BET surface areas of PAF-42, PAF-43, and PAF-42 are found to be 640 m^2 g^{-1}, 515 m^2 g^{-1} and 534 m^2 g^{-1}, respectively. Comparatively, the higher surface area of PAF-41 could be ascribed to the effect of electron-donating groups. In case of donating groups, the ability of ternary N atom is much stronger than of quaternary C, Si and Ge atoms, which would facilitate the polymerization process. In addition, the pore-size distributions of these materials are calculated according to the nonlocal density functional theory (NLDFT). To be specific, the pore parameters derived from the nitrogen isotherms are listed in Table 1. Although the structures of the resulting PAFs (PAF-42, PAF-43, and PAF-44) and the previous prepared PAFs (PAF-1, PAF-3, and PAF-4) using Yamamoto reaction seem similar, it is worth mentioning that the pore properties are different from each other. The PAFs in this study tend to possess smaller pore widths and lower BET surface area. Probably, the uncontrolled ortho and para substitutions, as well as different reaction types, would be responsible for this change.

For polymerization reaction, temperature plays a significant role in determining the properties of these polymers. The comparative experiments were conducted at 318 K and 333 K. As expectedly, the pore character of these polymers significantly varies with changing temperature (Figure 7 and Table S3). The surface areas of PAF-41, PAF-42, PAF-43, and PAF-44 increase with the rising reaction temperature from 318 K to 333 K. This is because the higher starting temperature would lead to more intense thermal motion which provides increasing opportunities for molecular collision. Therefore, with higher initial temperature, the monomers could be polymerized more quickly and effectively. Notably, the surface area of PAF-41 obtained at 333 K is 1119 m^2 g^{-1}, which is nearly double of that at 318 K. The sudden increase of the surface area could be elucidated by considering. Except for the reaction temperature effect, the electron-donating effect could enhance the activity of the initial monomer. In regards to that, the N atom of triphenylamine could offer electron-donating effect, which makes the monomer of PAF-41 more active than other monomers. Subsequently, the degree of polymerization increased, which might influence the BET surface area. Thus the surface area of PAF-41 based on triphenylamine shows a sudden increase compared with other PAFs in this study.

As the main components of greenhouse gas, the adsorptions of CO_2 and CH_4 are of significant importance to the social development in terms of clean energy and environmental issues. The porosity and high stability make PAFs ideal candidates for carbon dioxide and methane adsorption. The CO_2 and CH_4 adsorptions were studied at 273 K and 298 K, respectively. Figure 8 shows that the CO_2 and CH_4 uptakes of

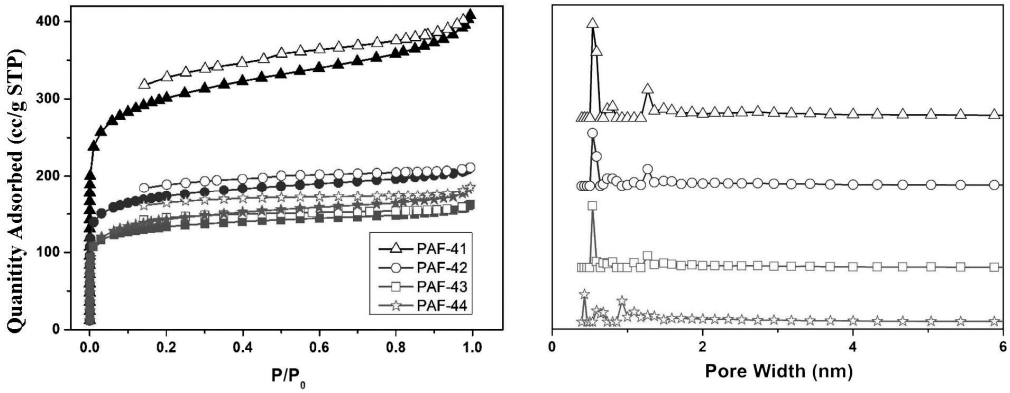

Figure 6. Experimental N_2 adsorption, desorption isotherms and pore width distribution of PAF-41 (triangle), PAF-42 (cycle), PAF-43 (square), and PAF-44 (star). STP = standard temperature and pressure. Pore size distributions were calculated by the NLDFT method.

PAF-41 are about 78.7 $cm^3 g^{-1}$ and 23.3 $cm^3 g^{-1}$ at 273 K, which are the highest among these samples. For clear illustration, the detailed

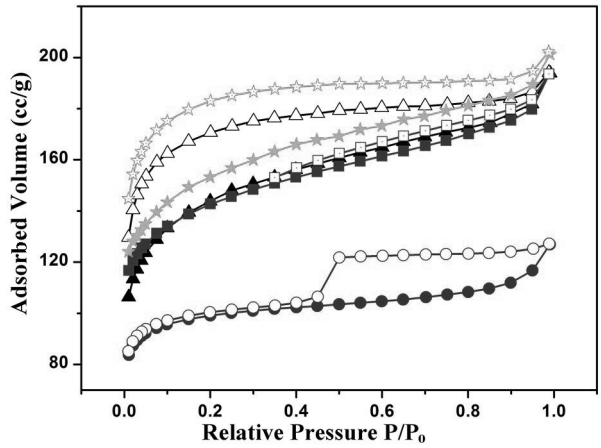

Figure 7. Experimental N_2 adsorption and desorption isotherms (77K) of PAF-41 (square), PAF-42 (cycle), PAF-43 (triangle), and PAF-44 (star) obtained at 318 K.

data of these materials are listed in Table 1. Even only with moderate surface areas ranging from 515 $m^2 g^{-1}$ to 1119 $m^2 g^{-1}$, the gas uptakes of these PAFs are not inferior to those of other POF materials. For example, PAF-1 with a large surface area (BET, 5600 $m^2 g^{-1}$) only possess the CO_2 uptake at 2.08 mmol g^{-1}, which is less than that of PAF-42 (2.47 mmol g^{-1}), let alone that of PAF-41 (3.52 mmol g^{-1}). The comparison of CO_2 and CH_4 uptakes between the obtained PAF materials and some representative POFs is listed in the Supporting Information (Table S4 and Table S5)[6,29-35].

In order to prove the affinity of guest molecules to host materials, the isosteric heat of adsorption (Q_{st}) was calculated based on the figures at 273 K and 298 K. Figure. 9 showed that PAF-43 possesses a larger CO_2 Q_{st} (34.8 kJ mol^{-1}) among the four PAF materials, which also surpassed plenty of previously reported POFs, such as PAF-1 (15.6 kJ mol^{-1}), PAF-3 (19.2 kJ mol^{-1})[29], MOP-A (23.7 kJ mol^{-1})[30], and CMP-1 (26.8 kJ mol^{-1})[31]. Similarly, resulting materials also exhibited an excellent performance in CH_4 uptakes, with Q_{st} reaching 29.8 kJ mol^{-1} for

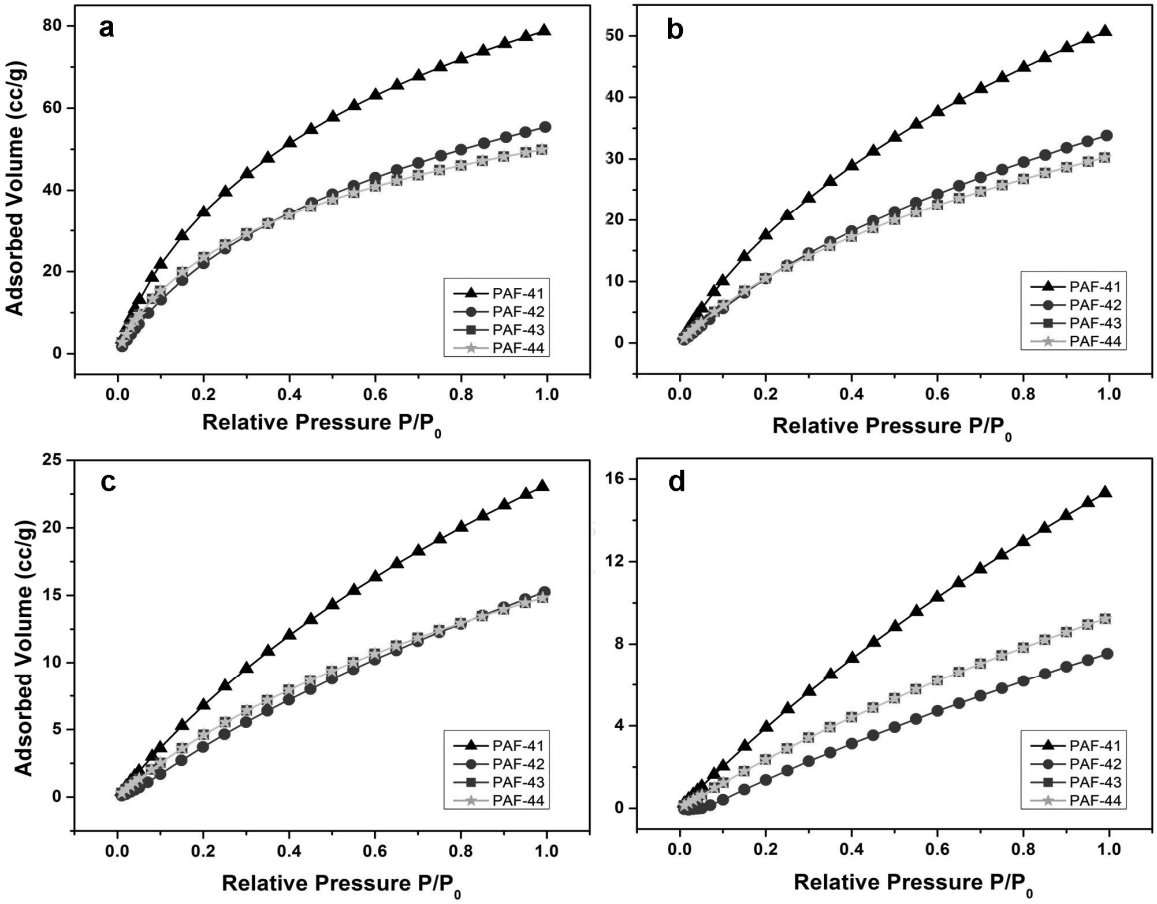

Figure 8. CO_2 adsorption isotherms of PAF-41 (triangle), PAF-42 (cycle), PAF-43 (square), and PAF-44 (star) at 273 K (a) and 298 K (b), as well as CH_4 isotherms at 273 K (c) and 298 K (d).

Journal Name

RSCPublishing

ARTICLE

Table 1. Porosity data and CO_2 and CH_4 uptake data of the PAFs (P/P_0=0.99)

PAFs	SA_{BET} [m^2/g]	Pore width [nm]	CO_2 uptake 273 K [mmol/g]	CO_2 uptake 298 K [mmol/g]	CH_4 uptake 273 K [mmol/g]	CH_4 uptake 298 K [mmol/g]	$Q_{st}CO_2$ [kJ/mol]	$Q_{st}CH_4$ [kJ/mol]
PAF-41	1119	0.56	3.52	2.26	1.04	0.68	28.1	17.0
PAF-42	640	0.51	2.47	1.51	0.68	0.34	31.8	25.6
PAF-43	515	0.57	2.17	1.24	0.60	0.28	34.8	29.8
PAF-44	532	0.46	2.23	1.35	0.67	0.41	34.2	22.9

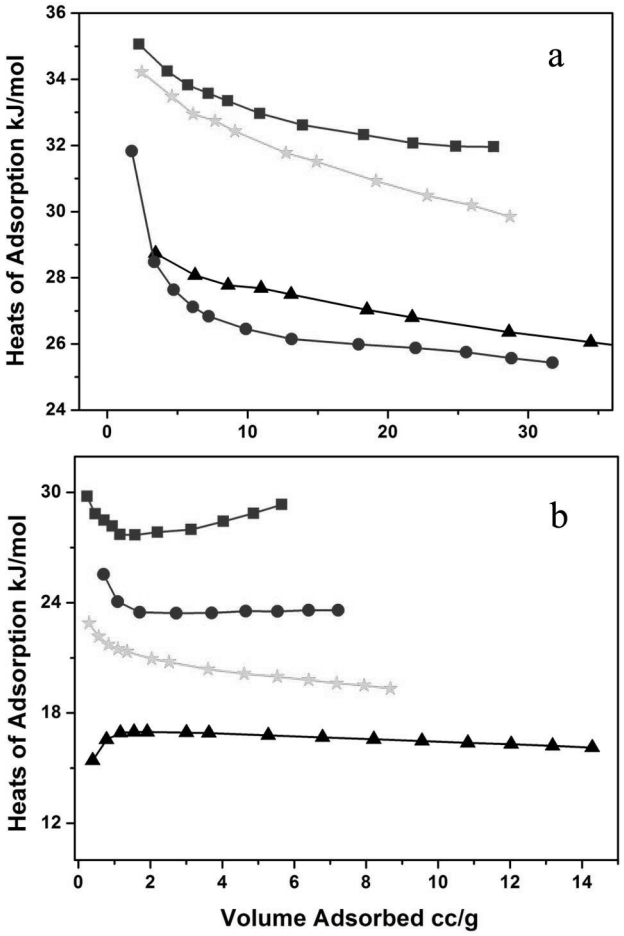

Figure 9. CO_2 (a) and CH_4 (b) isosteric heats of PAF-41 (triangle), PAF-42 (cycle), PAF-43 (square), and PAF-44 (star).

PAF-43 (Figure 9). Compared with some classic POFs, the CH_4 isosteric heat of adsorption (Q_{st}) of PAF-43 proves to be comparatively higher than that of PAF-1 (14.0 kJ mol^{-1})[29], PPF-1 (15.1 kJ mol^{-1})[32], and BILP-2 (18.4 kJ mol^{-1}).[33] Because of the similar structures of resulting PAFs (PAF-42, PAF-43, and PAF-44) with the previous PAFs (PAF-1, PAF-3, and PAF-4), their properties are analyzed and compared. The pore widths of PAF-1, PAF-3, and PAF-4 are 1.4 nm, 1.27 nm and 1.18 nm, respectively. Their corresponding isosteric heat of adsorptions for CH_4 followed a reverse pattern, at 14.0 kJ mol^{-1}, 15.0 kJ mol^{-1}, and 23.0 kJ mol^{-1}, which are averagely lower than those of PAF-42, PAF-43, and PAF-44[29,37]. It can be inferred that POF materials with smaller pore width are apt to possess higher isosteric heat of adsorptions. After careful catalysis, the specific networks with main pore size around 0.5 nm for the obtained PAFs probably promote the abilities of interaction between host materials and guest molecules (CO_2 and CH_4), which is responsible for their high Q_{st}. All the specific data and comparative results are listed in supporting information.

Conclusions

In summary, a low-cost and facile preparative strategy for PAF materials has been developed, which was successfully applied to synthesize a series of PAFs ,using inexpensive $AlCl_3$ as catalyst. The structure of these materials was well characterized and discussed. Based on N_2 sorption, various PAFs display a moderate surface areas ranging from 515 m^2 g^{-1} to 1119 m^2 g^{-1}, with uniform pore size distribution mainly centered at 0.5 nm. In addition, the resulting materials exhibited relatively high adsorption capacities for both CO_2 and CH_4. It is also worth noting that the new strategy addresses typical flaws of some classic PAFs, such as high cost and complexity of precursor preparation. We expect that this strategy can be utilized for mass production and provide opportunities for practical application in future.

Acknowledgements

We are grateful to the financial support from National Basic Research Program of China (973 Program, grant nos. 2012CB821700, 2014CB931804), Major International (Regional) Joint Research Project of NSFC (grant nos. 21120102034) and NSFC (21201074).

Notes and references

State Key laboratory of Inorganic Synthesis & Preparative Chemistry, Jilin University, Changchun, 130012, P. R. China

To whom correspondence should be addressed: E-mail: zhugs@jlu.edu.cn. Fax: +86-431-85168331; Tel: +86-431-85168331.

1. N. Mckeown and P. Budd, *Macromolecules*, 2010, **43**, 5163-5176.
2. R. Dawson, A. Cooper and D. Adams, *Prog. Polym. Sci.*, 2012, **37**, 530-563.
3. X. Zou, H. Ren and G. Zhu, *Chem. Commun.*, 2013, **49**, 3925-3936.
4. S. Ding and W. Wang, *Chem. Soc. Rev*, 2013, **42**, 548-568.
5. a) T. Ben, H. Ren, S. Ma, D. Cao, J. Lan, X. Jing, W. Wang, J. Xu, F. Deng J. Simmons and G. Zhu, *Angew. Chem. Int. Ed.*, 2009, **48**, 9457-9460; b) S. Kandambeth, D. Shinde, M. Panda, B. Lukose, T. Heine, R. Banerjee1, *Angew. Chem. Int. Ed.,* 2013, **52**, 13052–13056; c) B. Biswal, S. Chandra, S. Kandambeth, B. Lukose, T. Heine and R. Banerjee. *J. Am. Chem. Soc*., 2013, **135**, 5328−5331.
6. H. Furukawa and O. Yaghi, *J. Am. Chem. Soc.*, 2009, **131**, 8875-8883.
7. S. Ding, J. Gao, Q. Wang, Y. Zhang, W. Song, C. Su and W. Wang, *J. Am. Chem. Soc.*, 2011, **133**, 19816-19822.
8. X. Feng, L. Liu, Y. Honsho, A. Saeki, S. Seki, S. Irle, Y. Dong, A. Nagai and D. Jiang, *Angew. Chem. Int. Ed.*, 2012, **51**, 2618-2622.
9. a) N. McKeown, P. Budd, K. Msayib, B. Ghanem, H. Kingston, C. Tattershall, S. Makhseed, K. Reynolds and D. Fritsch, *Chem. Eur. J.*, 2005, **11**, 2610-2620; b) N. Mckeown, B. Ghanem, K. Msayib, P. Budd, C. Tattershall, K. Mahmood, S. Tan, D. Book, H. Langmi, A. Watlton, *Angew. Chem. Int. Ed.*, 2006, **45**, 2672-2676; c) M. Carta, R. Malpass-Evans, M. Croad, Y. Rogan, J. Jansen, P. Bemardo, F. Bazzarelli and N. Mckeown, *Science*, 2013, **319**, 303-307.
10. a) J. Jiang, F. Su, A. Trewin, C. Wood, N. Campbell, H. Niu, C. Dickinson, A. Ganin, M. Rosseinsky, Z. Khimyak and A. Cooper, *Angew. Chem. Int. Ed.*, 2007, **46**, 8574-8578; b) J. Jiang, F. Su, A. Trewin, C. Wood, H. Niu, J. Jones, Y. Khimyak and A. Cooper, *J. Am. Chem. Soc.*, 2008, **130**, 7710-7720; c) A. Cooper, *Adv. Mater.*, 2009, **21**, 1291-1295; d) R. Dawson, A. Laybourn, Y. Khimyak, D. Adams and A. Cooper, *Macromolecules*, 2010, **43**, 8524-8530.
11. a) C. Wood, B. Tan, A. Trewin, H. Niu, D. Bradshaw, M. Rosseinsky, Y. Khimyk, N. Campbel, P. Pirk, E. Stokel and A. Cooper, *Chem. Mater.*, 2007, **19**, 2034- 2048; b) C. Wood, B. Tan, A. Trewin, F. Su, M. J. Rosseinsky, D. Bradshaw, Y. Sun, L. Zhou and A. Cooper, *Adv.Mater.*, 2008, **20**, 1916-1921; c) Y. Luo, B. Li, W. Wang, K. Wu and B. Tan, *Adv. Mater.*, 2012, **24**, 5703-5707; d) S. Xu, Y. Luo and B. Tan, *Macromol. Rapid. Commun.*, 2013, **34**, 471-474.
12. P. Kuhn, M. Antonietti and A. Thomas, *Angew. Chem. Int. Ed.*, 2008, **47**, 3450-3453.
13. S. Ren, M. Bojdys, R. Dawson, A. Laybourn, Y. Khimyak, D. Adams and A. Cooper, *Adv. Mater.*, 2012, **24**, 2357-2361.
14. a) H. Ren, T. Ben, E. Wang, X. Jing, M. Xue, B. Liu, Y. Cui, S. Qiu and G. Zhu, *Chem. Commun.*, 2010, **46**, 291-293; b) H. Ren, T. Ben, F. Sun, M. Guo, X. Jing, H. Ma, K. Cai, S. Qiu and G. Zhu, *J. Mater. Chem.*, 2011, **21**, 10348-10353; c) H. Zhao, Z. Jin, H. Su, J. Zhang, X. Yao, H. Zhao and G. Zhu, *Chem. Commun.*, 2010, **49**, 2780-2782; d) S. Garibay, M. Weston, J. Mondloch, Y. Colon, O. Farha, J. Hupp, S. Nguyen, *CrystEngComm.*, 2013, **15,** 1515-1519.
15. a) C. Shen, Y. Bao, Z. Wang, *Chem. Commun.*, 2013, **49**, 3321-3323; b) H. Yu, M .Tian, C. Shen, and Z Wang, *Polym. Chem.*, 2013, **4**, 961-968.
16. J. Colson, and W. Dichtel, *Nat. Chem.*, 2013, **5**, 453.
17. a) Y. Zhang and S. Riduan, *Chem. Soc. Rev.*, 2012, **41**, 2083-2094; b) S. Yuan, J. Shui, L. Grabstanowisz, C. Chen, S. Commet, B. Reprogle, T. Xu, L. Yu and D. Liu, *Angew. Chem. Int. Ed.*, 2013, **52**, 8349-8353; c) K. Tanabe, N. Siladke, E. Broderick, T. Kobayashi, J. Goldston, M. Weston, O. Farha, J. Hupp, M. Pruski. E. Mader, M. Johoson and S. Nguyen, *Chem. Sci.*, 2013, **4**, 2483–2489; d) R. K. Totten, M. Weston, J. Park, O. Farha, J. Hupp and and S. Nguyen, *ACS Catal.*, 2013, **3**, 1454-1459; e) L. Stegbauer, K. Schwinghammer, B. Lotsch, *J. Am. Chem. Soc.*, 2013, 135, 17853–17861.
18. Y. Yuan, H. Ren, F. Sun, X. Jing, K. Cai, X. Zhao, Y. Wang, Y. Wei and G. Zhu, *J. Mater. Chem.*, 2012, **22**, 24558-24562.
19. Z. Xiang and D. Cao, *Macromol. Rapid. Commun.*, 2012, **33**, 1184-1190.
20. X. Feng, L. Chen, Y. Honsho, O. Saengsawang, L. Liu, L. Wang, A. Saeki, S. Irle, S. Seki, Y. Dong and D. Jiang, *Adv. Mater.*, 2012, **24**, 3026-3031.
21. J. Weber and A. Thomas, *J. Am. Chem. Soc.*, 2008, **130**, 6334-6335.
22. J. Schmidt, M. Werner and A. Thomas, *Macromolecules*, 2009, **42**, 4426-4429.
23. a) S. Yuan, B. Dorney, D. White, S. Kirklin, P. Zapol, L. Yu and D. Liu, *Chem. Commun.*, 2010, **46**, 4547-4549; b) M. Weston, O. Farha, B. Hauser, J. Hupp and S. Nguyen, *Chem. Mater.*, 2012, **24**, 1292-1296.
24. a) Q. Chen, M. Luo, P. Hammershøj, D. Zhou, Y. Han, B. Laursen, C. Yan and B. Han, *J. Am. Chem. Soc.*, 2012, **134**, 6084-6087; b) Q. Chen, D. Liu, M. Luo, L. Feng, Y. Zhao and B. Han, *Small*, 2013, **10**, 308-315.
25. a) R. Dawson, T. Ratvijitvech, M. Corker, A. Laybourn,Y. Khimyak, A. Cooper and D. Adams, *Polym. Chem.*, 2012, 3, 2034; b) R. Dawson, L. Stevens, T. Drage, C. Snape, M. Smith, D. Adams, and A. Cooper, l*J. Am. Chem. Soc.*, 2012, **134**, 10741−10744; c) Y. Luo, B. Li, W. Wang, K. Wu , and B. Tan, *Adv. Mater.*, 2012, **24**, 5703-5707; d) B. Li, R. Gong, W. Wang, X. Huang, W. Zhang, H. Li, Ch. Hu, and B. Tan, l*Macromolecules* 2011, **44**, 2410–2414.
26. a) P. Kovacic and R. Lange, *J. Org. Chem.*, 1964, **29**, 2416-2420; b) E. Mughal and D. Kuck, *Chem. Commun.*, 2012, **48**, 8880–8882; c) P. Kovacic and A. Kyriakis, *J. Am. Chem. Soc.*, 1963, **85**, 454-458; d) B. King , J. Kroulik , C. Robertson , P. Rempala , C. Hilton , J. Korinek , and L. Gortari, *J. Org. Chem.*, 2007, **72**, 2279–2288; e) L. Zhai, R. Shukla, R. Rathore, *Org. let.*, 2009, **11**, 3474-3477.
27. M. Grzybowski, K. Skonieczny, H. Butenschön and D. Gryko, *Angew. Chem. Int. Ed.*, 2013, **52**, 9900-9930.
28. O. Farha, A. Spokoyny, B. Hauser, Y. Bae, S. Brown, R. Snurr, C. Mirkin and J. Hupp, *Chem. Mater.*, 2009, **21**, 3033-3035.
29. T. Ben, C. Pei, D. Zhang D, J. Xu, F. Deng, X. Jing and S. Qiu, *Energy. Environ. Sci.*, 2011, **4**, 3991-3999.
30. R. Dawson, E. Stöckel, J. Holst, D. Adams and A. Cooper, *Energy. Environ. Sci.*, 2011, **4**, 4239-4245.
31. R. Dawson, D. Adams and A. Cooper, *Chem. Sci.*, 2011, **2**, 1173-1177.
32. Y. Zhu, H. Long and W. Zhang, *Chem. Mater.*, 2013, **25**, 1630-1635.
33. M. Rabbani and H. El-Kaderi, *Chem. Mater.*, 2012, **24**, 1511-1517.
34. M. Rabbani, T. Reich, R. Kassab, K. Jackson and H. El-Kaderi, *Chem. Commun.*, 2012, **48**, 1141-1143.
35. H. Ma, H. Ren, X. Zou, F. Sun, Z. Yan, K. Cai, D. Wang and G. Zhu, *J. Mater. Chem. A*, 2013, **1**, 752-758.

36. J. Mendoza-Corte´s, S. Han, H. Furukawa, O. Yaghi and W. Goddard, *J. Am. Chem. Soc.*, 2008, **35**, 11580–11581.

37. Y. Zhang, B. Li, K. Williams, W. Gao and S. Ma, *Chem. Commun.*, 2013, **49**, 10269.

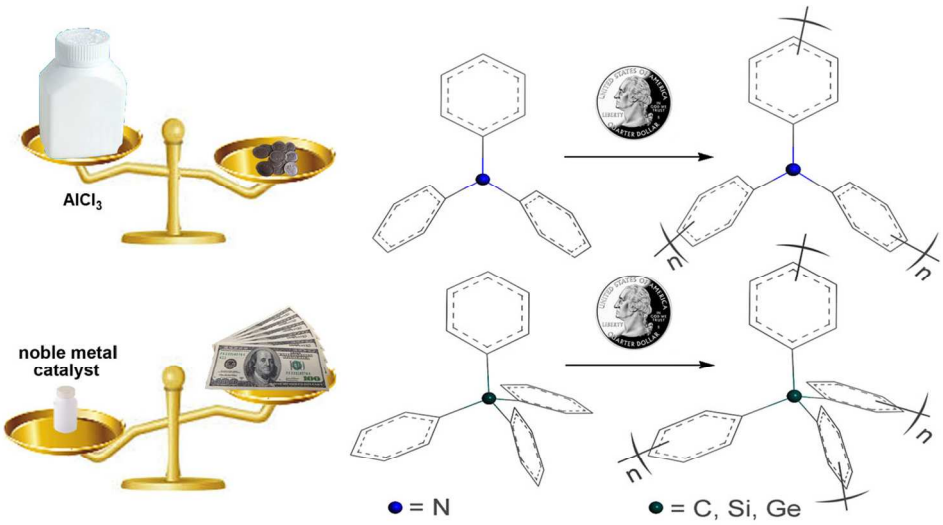

119x65mm (300 x 300 DPI)